Chemical Engineering Research and Design 206 (2024) 175–187

Contents lists available at ScienceDirect

Chemical Engineering Research and Design

journal homepage: www.elsevier.com/locate/cherd

Synthesis of robust interface-anchored composite PVA/PSU/epoxy membrane for highly efficient pervaporation in concentrated brine desalination

Thi Thi Mar [a], Yunlong Xue [a], Jiahua Yan [b], Zijian Yu [b], Bing Cao [a,*], Rui Zhang [b,c,**]

[a] College of Materials Science and Engineering, Beijing University of Chemical Technology, Beijing 100029, China
[b] College of Chemical Engineering, Beijing University of Chemical Technology, Beijing 100029, China
[c] National-Local Joint Engineering Research Center Of Biomass Refining and High-Quality Utilization, Changzhou 213164, China

ARTICLE INFO

Keywords:
Pervaporation desalination
Composite membrane
Polysulfone
Bisphenol A

ABSTRACT

This study investigates the enhancement of peel-off resistance in polysulfone (PSU) membranes through the incorporation of bisphenol-A. The modified membranes were fabricated and characterized to evaluate their performance compared to conventional PSU membranes. Enhancing the interlayer adhesion within the composite membrane stands as a pivotal factor for ensuring its stable operation. Through meticulous characterization of the PSU structure and surface properties, our findings underscore the significant enhancement in interlayer adhesion facilitated by the introduction of bisphenol-A. In addition, we demonstrate the synergistic effects of PVP and SPSF additives in enhancing the hydrophilic nature of PSU membranes and the development of a novel active layer for membranes by incorporating 1.5 wt% polyvinyl alcohol with P(SS-MA) crosslinker on a PSU supporting layer. The synergistic effects of PVA and P(SS-MA) crosslinker contribute to improved salt rejection while maintaining structural integrity. Operating at a temperature of 70 ℃ and with a 3.5 wt% NaCl aqueous solution, the 16:1 membrane coated with a PVA/P(SS-MA) coating layer exhibited a remarkable flux of 53.6 ± 9.8 kg m^{-2} h^{-1}. Moreover, treating a highly concentrated solution of 10 wt% at the same temperature yielded a high flux of 38.73 ± 7.4 kg m^{-2} h^{-1}. Our findings underscore the potential of bisphenol-A modified PSU membranes as promising candidates for applications where strong adhesion and durability are paramount.

1. Introduction

Water scarcity is a consequence of the world's rapidly increasing population, climate change, the development of agricultural production, and industrialization (Kılıç, 2020; Tzanakakis et al., 2020). Desalination of seawater and brackish water using different membrane types, such as ceramic, polymeric, and composite membranes, is an essential remedy for the water problem (Halakoo and Feng, 2020). The two primary desalination methods are membrane-based and thermal (phase change) (Li et al., 2017). Because membrane technology has high operational stability, low chemical costs, ease of fabrication, and ease of maintenance within industrial processes, it has received extensive study and industrial use in a variety of fields (Julian et al., 2022; Zeng et al., 2020). The liquid phase feed and the vapor phase permeate are two separate phases that make up the pervaporation process (Kavanagh et al., 2009). These two phases are separated by the membranes, which act as a selective barrier (Cho et al., 2011). Additionally, they allow the desired components of the liquid feed to vaporize through them. Reverse osmosis (RO) accounts for about 60 % of the desalination market due to its advantages of low energy consumption, low equipment investment, and high effluent quality (Lee et al., 2011). However, the rapid increase in the cost of reverse osmosis at high osmotic pressures makes it impossible to desalinate concentrated brine (Lim et al., 2021). Pervaporation technology offers a variety of advantages, including ease of use and great utility for temperature-sensitive compounds (Kaminski et al., 2018; Ong et al., 2016). Membrane fouling, reduced membrane stability, decreased water flux, and low permeate flow rates at low temperatures are the main drawbacks of pervaporation technology (Wang et al., 2016; Zhao et al., 2020).

Pervaporation membranes, in particular, are frequently used in

* Corresponding author.
** Corresponding author at: College of Chemical Engineering, Beijing University of Chemical Technology, Beijing 100029, China.
E-mail addresses: bcao@mail.buct.edu.cn (B. Cao), zhangrui1@mail.buct.edu.cn (R. Zhang).

https://doi.org/10.1016/j.cherd.2024.04.052
Received 21 February 2024; Received in revised form 9 April 2024; Accepted 24 April 2024
Available online 26 April 2024

Table 1
Composition of the PSU dope solution for the substrate layer.

PSU	SPSF	PVP	NMP
12 wt%	2 wt%	10 wt%	76 wt%

Table 2
Composition of dope solution for the separation layer.

PVA	P(AA-AMPS)	P(SS-MA)
1.5 wt%	30 wt%	1 wt%

membrane-based separation technology to produce ultra-pure water (An et al., 2014). This is a result of the straightforward manufacturing procedures, minimal energy needs, and high thermal and mechanical strengths of these membranes (Kim et al., 2015). Because of the PV membrane's ease of water molecule passage from the feed side, the condenser's capacity to collect permeate vapor onto the permeate side (Eljaddi et al., 2021; Yang et al., 2020). PV membranes with dense layers are used in the desalination process due to their benefits, which include low cost, high-energy effectiveness, high salt rejection, and minimal fouling. Membranes with the hydrophilic ability to move through water molecules with ease (Xie et al., 2011). The composition of the separation layer influences how easily the membrane can split. The separation layer also affects the membrane-transport properties (Guo et al., 2008). Foulants, or the deposition of specific particles on the membrane surface during the pervaporation process, such as colloids and suspended particles, are to be held responsible for decreased penetration and salt rejection (Park et al., 2014). Despite being widely used for a variety of applications, epoxy resin cannot withstand heat stability despite having excellent bonding performance, strong adhesive strength, and coating (Gargol et al., 2021; Jin et al., 2015).

In this study, we examined the efficacy of polysulfone (PSU) membranes and explored the impact of various organic additives, namely bisphenol A, polyvinylpyrrolidone (PVP), propionic acid (PA), and sulfonated polysulfone (SPSF). Due to its excellent chemical resistance, high mechanical strength., and good thermal stability, polysulfone material was chosen as the support layer (Chaudhri et al., 2018; Madaeni and Rahimpour, 2005). PVA materials are easily crosslinked with P(SS-MA), resulting in a dense hydrophilic membrane that is highly durable and suitable for water-selective permeation (Burts et al., 2022). In addition, poly(vinylpyrrolidone) (PVP) is soluble in water, it is often studied as a pore-forming agent (Al Malek et al., 2012). With the addition of PVP, the porosity and number of pores of the produced membranes increased (Acarer, 2022). Due to its superior physical and chemical properties, such as high oxidation stability and thermal stability, SPSF is often used as a hydrophilic membrane material (Hu et al., 2021). To enhance the functionality of the PSU membrane, in this work, propionic acid (PA) was added as a non-solvent addition to the casting solution (Han, 1999). Maintaining the adhesion of the separation layer to the substrate layers is crucial when employing PV thin film composite membranes for desalination. To address this concern, epoxy resin, synonymous with bisphenol A, was selected as the foundational membrane material due to its cost-effectiveness, ease of synthesis, and high physiochemical stability. To enhance resistance to peeling, a small quantity of epoxy resin (bisphenol-A) was incorporated into the PSU-based solution in this experiment. The involvement of bisphenol A in the supporting membrane was meticulously investigated. The resulting PSU/epoxy composite membranes demonstrated improved resistance to peeling and exhibited high flux values.

2. Experimental

2.1. Materials

Polysulfone (PSU-3050) was provided by Solvay S.A Co., Ltd. Sulphonated polysulfone (SPSF) (15 % sulphonation) was obtained from Shandong Jinlan. N-methyl-2-pyrrolidone (NMP, purity > 99.0 %) and 98 % by weight of sulfuric acid (H_2SO_4), triethanolamine (TEA), and 1,6-hexamethylenediamine (HMDA) were purchased at Tianjin Da Mao Chemical Reagent Factory (China). NMP was dried using the 4 Å molecular sieve. Propanoic acid (PA, Mw: 74 g/mol) was obtained from the Tianjin Fuchen Chemical Reagent Plant (China). Polyvinylpyrrolidone (PVP, K-30, Mn: 44,000–54,000) and epoxy resin (Bisphenol-A) were sourced from Gongbike New Material Technology Co., Ltd. Polyethylene terephthalate (PET) non-woven fabric was supplied from Shanghai Pole Technology Co., Ltd. Polyvinyl alcohol (PVA, Mw: 104,000 g/mol, 99.4 % hydrolysis), poly (4-styrene sulfonic acid-co-maleic acid) sodium salt (P(SS-MA), Mw: 20,000), poly acrylic acid co-2-acrylamido-2-methyl propane sulfonic acid (P(AA-AMPS), Mw: 2000–5000 g/mol) and sodium chloride (NaCl, purity > 99.9 %) were bought from Sinopharm Chemical Reagent Co., Ltd. (China). Deionized water was obtained using a laboratory-equipped Millipore ultrapure water system from our laboratory.

2.2. Membrane preparation

2.2.1. Preparation of dope solution

The preparation method for the dope solution of the substrate layer is

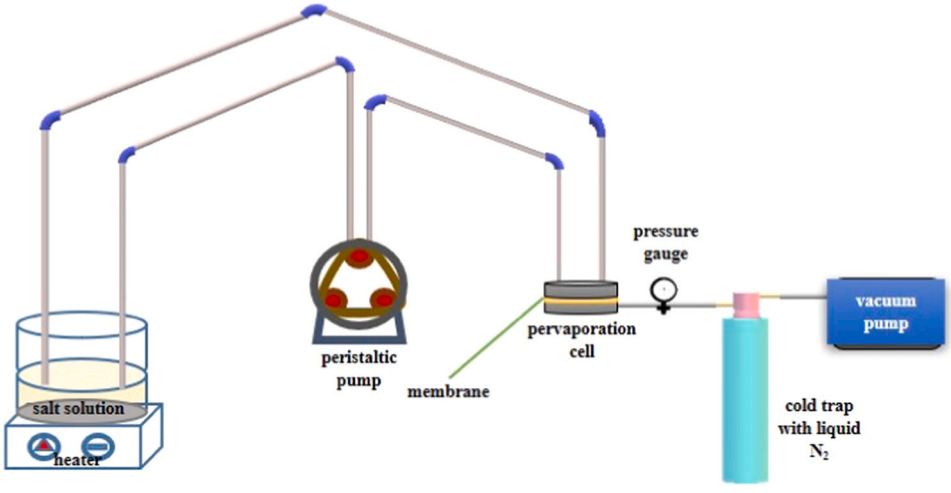

Fig. 1. The diagrammatic sketch of the pervaporation set up.

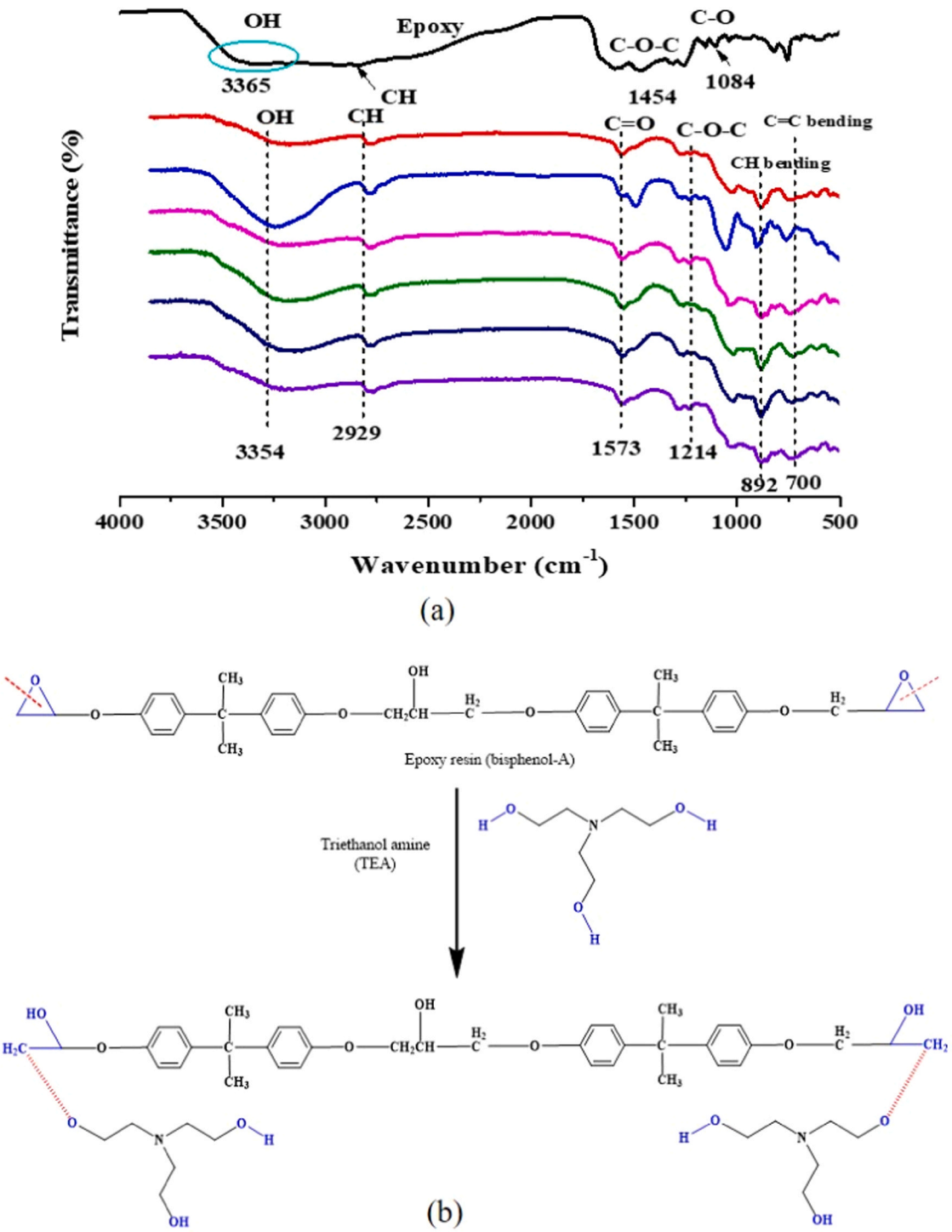

Fig. 2. FTIR spectrum (a) and chemical reaction formula (b) under blending conditions of different ratios of PSU and triethanolamine (TEA)/epoxy.

as follows: PSU, SPSF, PVP, and NMP were mixed and the composition of the dope solution of the substrate layer was shown in Table 1. The mixture components were stirred in the flask at room temperature for 12 h to obtain a homogeneous transparent solution. Then, 5 mL of propanoic acid (PA) and bisphenol-A were dissolved in dope solution by mild stirring to obtain a homogeneous transparent solution. Then, add 2 mL of triethanolamine or 1,6-hexamethylene diamine and continue stirring until the solution returns to homogeneous transparent.

The preparation method for the dope solution of the separation layer is as follows: PVA solution was mixed with the P(AA-AMPS) and P(SS-MA) crosslinkers respectively until to reach the weight ratio of 7:3, and then the resulting mixture was acidified to reach pH 1 using the H_2SO_4. In addition, the composition of dope solution for the separation layer was shown in Table 2.

2.2.2. *Preparation of substrate and composite membranes*

The coating of PSU/epoxy resin solution on the PET non-woven was applied with a 200 μm coating knife at room temperature. The coated membrane was introduced into the coagulation bath which contained deionized water and the phase inversion occurred. The deionized water in the coagulation bath was changed every 12 h to ensure that all traces of the solvent and additives were removed. The supporting membrane

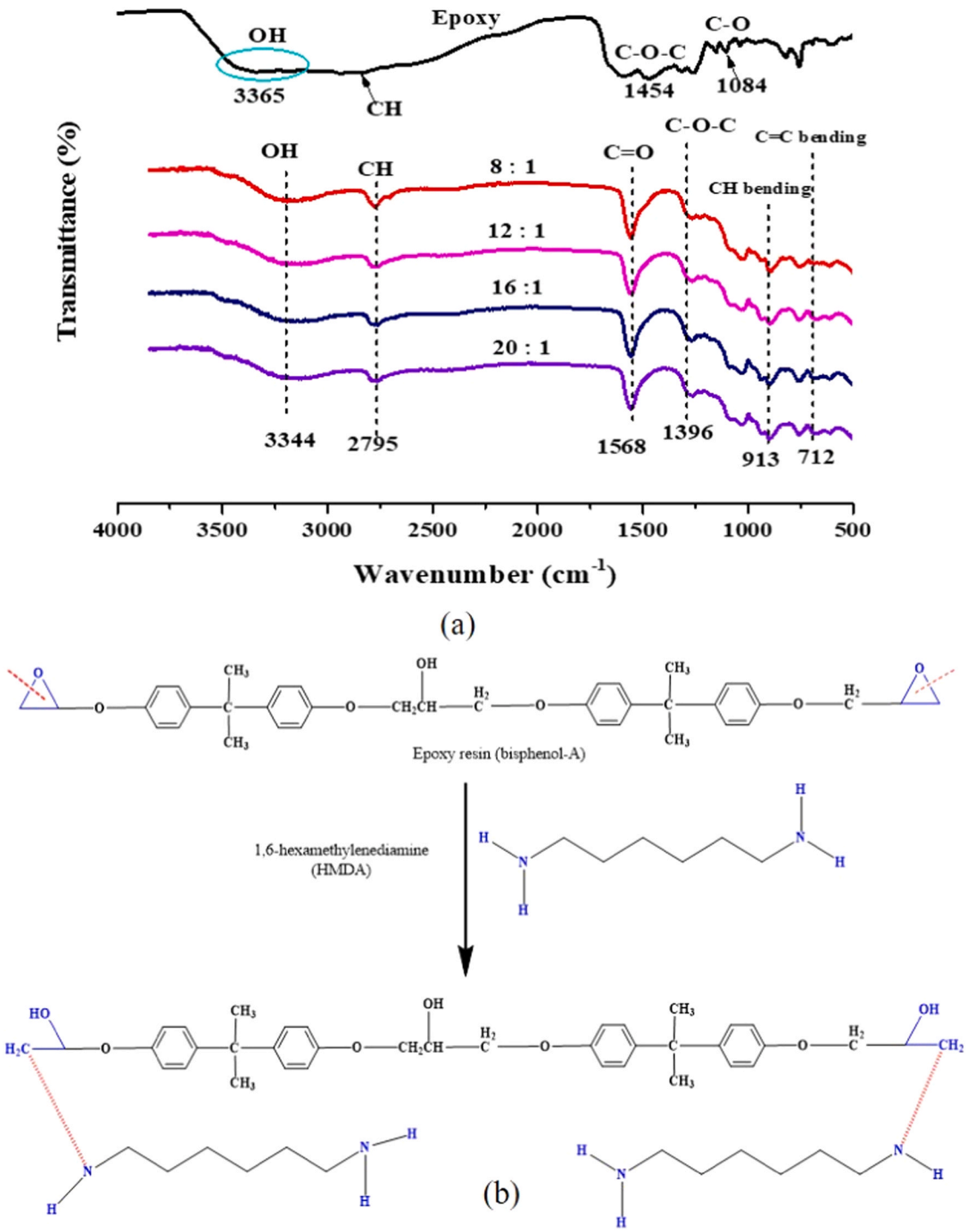

Fig. 3. FTIR spectrum (a) and chemical reaction formula (b) under blending conditions of different ratios of PSU and 1,6-hexamethylenediamine (HMDA)/epoxy.

was removed from the coagulation bath and dried in air for 24 h at room temperature.

The pervaporation composite membrane was made by spray-coating the coating solution with an airbrush on a supporting membrane. The air pressure was kept between 0.2 and 0.4 MPa, and the airbrush's nozzle was placed 0.15 m from the membrane's surface. The thickness of the membrane layer was changed by varying the spraying rate. The composite membrane naturally dried in air, and then placed in an oven for thermal crosslinking at 100 ℃ for 15 min. The composite membrane was made using the method shown in Supplementary Figure 1.

2.3. Characterizations of membrane properties

Several techniques and instruments were used to characterize the substrate and composite membranes. The surface and cross-section morphologies of the composite membranes consisting of PVA/PSU/epoxy (TEA) and PSU/epoxy (TEA) substrate layers were investigated utilizing a thermal field emission scanning electron microscope (SEM, JSM-7800 F, JEOL Ltd, Japan). Atomic force microscope (AFM, Dimension Fastscantm, Bruker, USA) was used to measure the surface roughness of the membranes. Fourier transform infrared spectroscopy (ATR-FTIR, Nicolet 560) was used to analyze the bonding between the

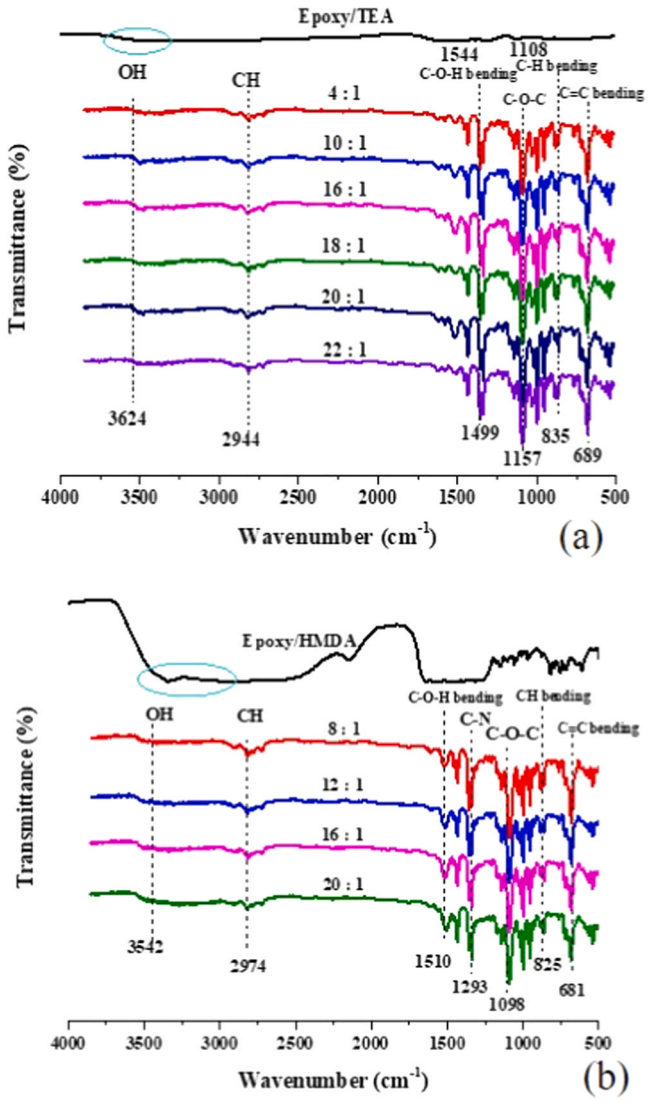

Fig. 4. FTIR spectra of the reaction between PVA and crosslinking agents (a) P (AA-AMPS) and (b) P(SS-MA).

PVA and PSU/epoxy membranes. The composites' ATR-FTIR spectra were measured in the 500 cm^{-1} - 4000 cm^{-1} wavenumber range. Thermogravimetric analysis (TGA, instrument model TA Q 100, USA) was conducted in a nitrogen atmosphere (100 mL/min) at a heat rate of 10 ℃/min to characterize the thermal properties of pristine PVA and PVA/P(SS-MA).

2.4. Hydrophilicity test of membrane

Water contact angle goniometer (CA) (DSA 100, KRUSS, Germany) was used to measure the wettability of PSU/epoxy membranes and PVA/PSU/epoxy composite membranes. On the flattened membrane surface, a drop of deionized water was dropped. A camera was used to take the image. The water contact angle of each sample was measured at least five times, and the average value was then calculated.

2.5. Ultrafiltration and gas permeation tests

A dead-end ultrafiltration apparatus (Supplementary Figure 2) was used to evaluate the ultrafiltration capabilities of PSU/epoxy-based membranes. The effective membrane area was 1.26×10^{-3} m^2. The membrane was installed in the cell of the dead-end ultrafiltration apparatus. It was initially compressed at a pressure of 0.3 MPa for a duration of 30 min. The water flux was then measured 5 times at room temperature. The following Eq. (1) was used to calculate the flux value.

$$J = \frac{M}{A_1 \times T_1} \quad (1)$$

A_1 was the effective membrane area (m^2), J was the permeate flux (kg/ m^2.h), M was the collected water (kg) and T_1 was the operation period (h).

The gas permeation cell was used to determine the PSU membrane's gas transport resistance (Supplementary Figure 3). The effective area was 0.95×10^{-4} m^2. The gas permeation cell would typically operate at high transmembrane pressures to record a series of N_2 measurements. Gas permeability can be used to calculate the average pore size and porosity of the membrane. After that, the correlation between the transmembrane pressure and gas flux could be determined using Eq. (2):

$$Q = \frac{V}{A \times T} \quad (2)$$

A was the effective membrane area (m^2), Q was the gas flux of N_2 (kg/ m^2.h), V was the volume of gas (L), and T was the data collection time (h).

2.6. Pervaporation desalination test

A bespoke pervaporation apparatus (Fig. 1) was utilized to assess the desalination efficacy of the PSU-based composite membranes. A PSU-based composite membrane was positioned atop the porous metal plate within the bespoke pervaporation apparatus. The actual working area of the composite membrane was 3.14 cm^2. A constant pressure of 100 Pa was maintained on the permeable side of the membrane. A feed solution containing a 3.5 wt% NaCl salt solution was employed on the feed side of the membrane at 70 ℃. Both the feed solution and the permeate solution had their conductivity measured using a Thermo Fish OAKTON, Con 110 Singapore conductivity meter. The liquid vapor produced on the permeate side was gathered using the liquid nitrogen cold trap over a minimum of four operations, each lasting around ten minutes. The following Eq. (3) was used to calculate the water flux (J value):

$$J = \frac{M}{s_1 \cdot t_1} \quad (3)$$

where J was the water flux (kg/ (m^2 h)), M was the collected water in a cold trap by permeate side (kg), s_1 was the effective membrane area (m^2) and t_1 was the operation time (h). Salt rejection (R_{NaCl}, %) of sodium chloride was measured using the following Eq. (4):

$$R_{NaCl} = \frac{C_{feed} - C_{permeate}}{C_{feed}} \times 100\% \quad (4)$$

where, C_{feed} was the salt concentration of the feed solution (m S cm^{-1}) and $C_{permeate}$ was the salt concentration of the permeate solution (m S cm^{-1}).

3. Results and discussion

3.1. Characterization of substrate layer and separation layer

PSU and epoxy are both polymers with a copolymerized unit structure containing bisphenol A in their main chains, thereby exhibiting excellent mutual solubility characteristics. Mixing the two polymers in different ratios, and using TEA and HMDA as crosslinking agents to crosslink the epoxy resin separately, forms a spatially interlocked crosslinked structure with PSU. This contributes to enhancing the stability of the substrate layer structure. Ammonia hydroxyl group-containing catalysts can expedite the crosslinking process of epoxy

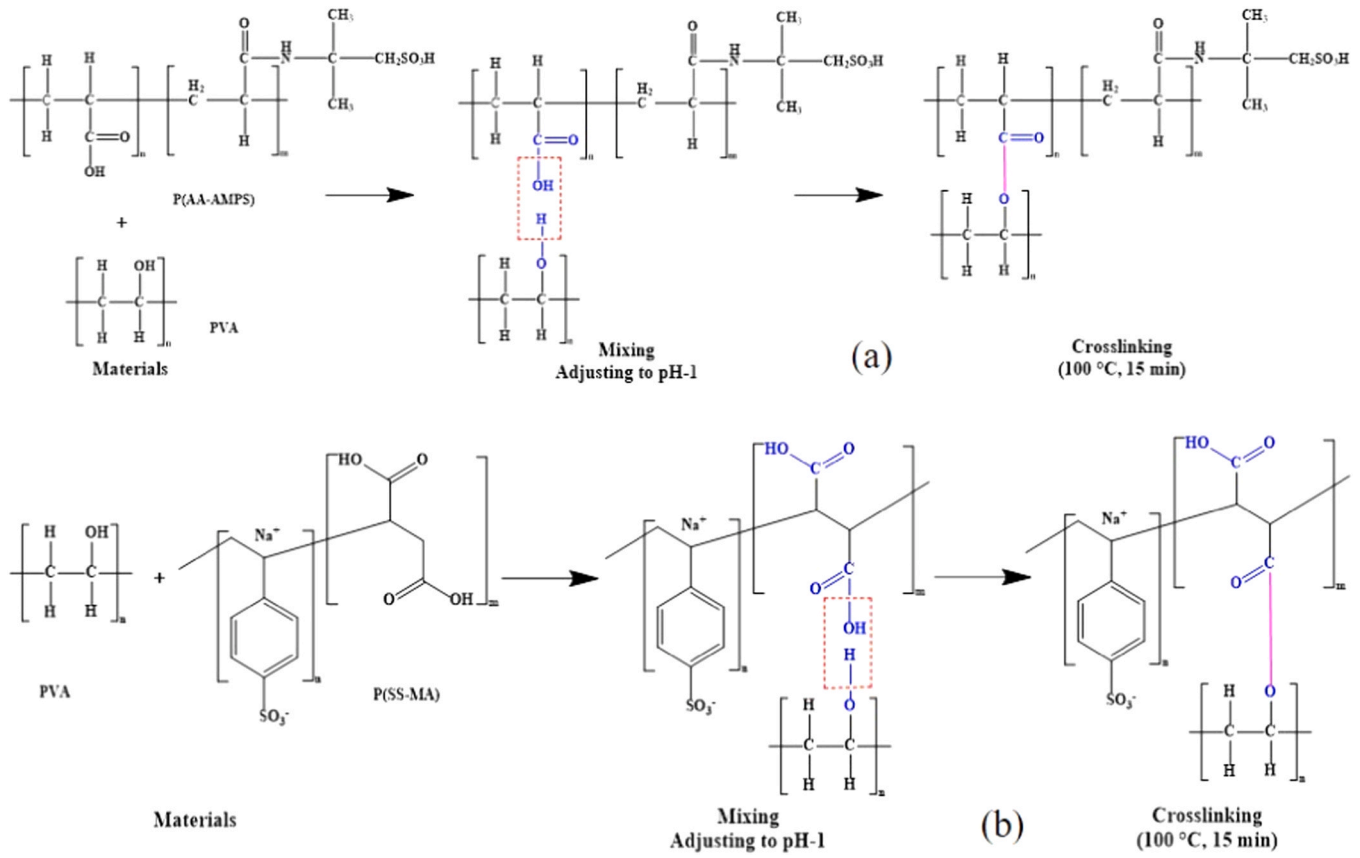

Fig. 5. Molecular reaction equations of the reaction between PVA and crosslinking agents (a) P(AA-AMPS) and (b) P(SS-MA).

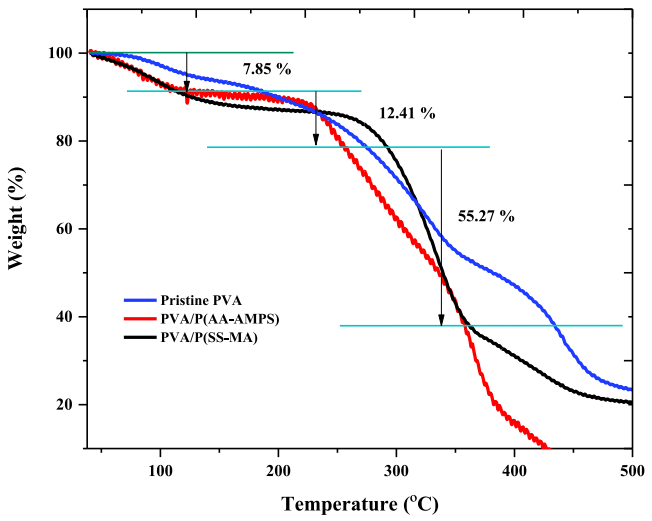

Fig. 6. TGA curve of PVA, PVA/P(AA-AMPS) and PVA/P(SS-MA) membranes under nitrogen atmosphere.

resins. Catalyst has the ability to split open epoxide rings and create a bridge to crosslink polymer chains. The structure of the PSU/epoxy (TEA) and PSU/epoxy (HMDA) substrate layers and composite membranes were investigated using the FTIR technique. The peaks having the range from 3300 cm^{-1} to 3400 cm^{-1} and from 2900 cm^{-1} to 3000 cm^{-1}, respectively, expressed the functional groups containing the -OH stretching frequency and $–CH_2$ stretching frequency parts (Mansur et al., 2008; Zhao et al., 2020). Peaks of the C═O stretching frequency, C–O stretching frequency, C–H bending vibration, and C═C bending vibration was detected about at between 1500 cm^{-1} to 1600 cm^{-1}, between 1200 cm^{-1} to 1400 cm^{-1}, about 900 cm^{-1}, and about 700 cm^{-1} (Guo et al., 2008). From the FTIR spectra, it can be observed that the introduction of amino crosslinking agents with both bifunctional and trifunctional groups result in new absorption peaks. Moreover, as the proportion of epoxy resin increases, the height of the absorption peaks continuously strengthens. This demonstrates that the incorporation of different amino groups in the system can lead to the curing and crosslinking of epoxy resin, forming a homogeneous interpenetrating network structure with PSU in the substrate layer. The stretching vibration absorption peak of N-H overlaps with the -OH peak, making it indistinguishable. However, the bending vibration of N-C produces an absorption peak in the range of nearly 1230 cm^{-1}, as clearly seen in Fig. 2(a) and Fig. 3(a). It is evident that a pronounced absorption peak appears after crosslinking of the epoxy resin. This indicates that the introduced multifunctional amino groups undergo crosslinking reactions in the blended system. Explaining the Fourier Transform Infrared Spectroscopy (FTIR) data of epoxy resin with triethanolamine (TEA) and hexamethylenediamine (HMDA) involves interpreting the spectra to identify characteristic peaks corresponding to chemical functional groups and understanding how the presence of TEA and HMDA affects the epoxy resin. Epoxy resin typically contains epoxide (C–O–C) groups, while TEA and HMDA contain amine (N–H) groups. The stretching frequency about 1454 cm^{-1} showed the C–O–C peak of epoxide group and then the peak between 2800 cm^{-1} - 3100 cm^{-1} indicated the stretching vibration of C–H. The primary reaction between epoxy resin with TEA or HMDA involves the opening of the epoxide ring by the amine group of TEA or HMDA. This results in the formation of hydroxyl groups (–OH) and amine adducts. Moreover, the C–O–C peak of epoxide group change to the broad peak and appeared at about 1500 cm^{-1}, indicating ring opening.

After preparing a stable substrate layer, we applied PVA to create a

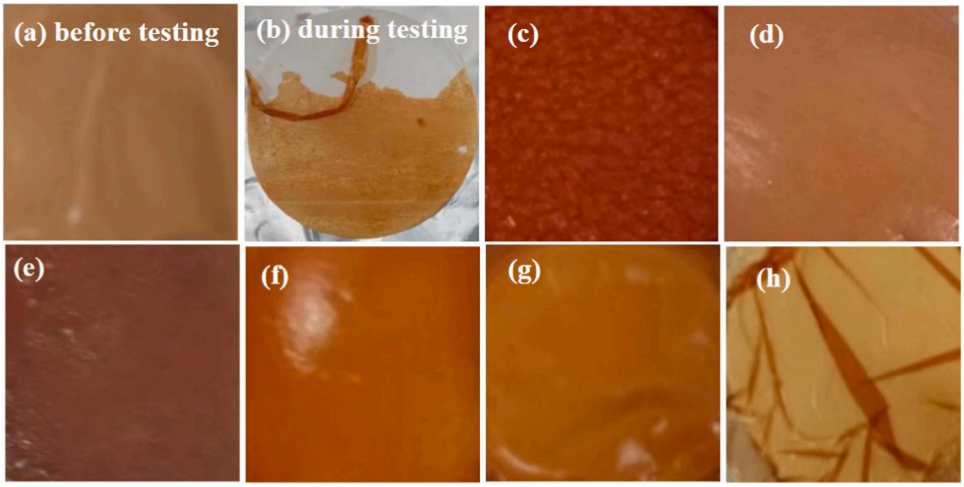

Fig. 7. Surface image of PVA/PSU composite membranes without epoxy resin: (a) before PV desalination and (b) during PV, and surface images of PVA/PSU/epoxy (TEA) ratios of (c) 4:1, (d) 10:1, (e) 16:1, (f) 18:1, (g) 20:1, and (h) 22:1 after desalination performance at 70°C (1 h).

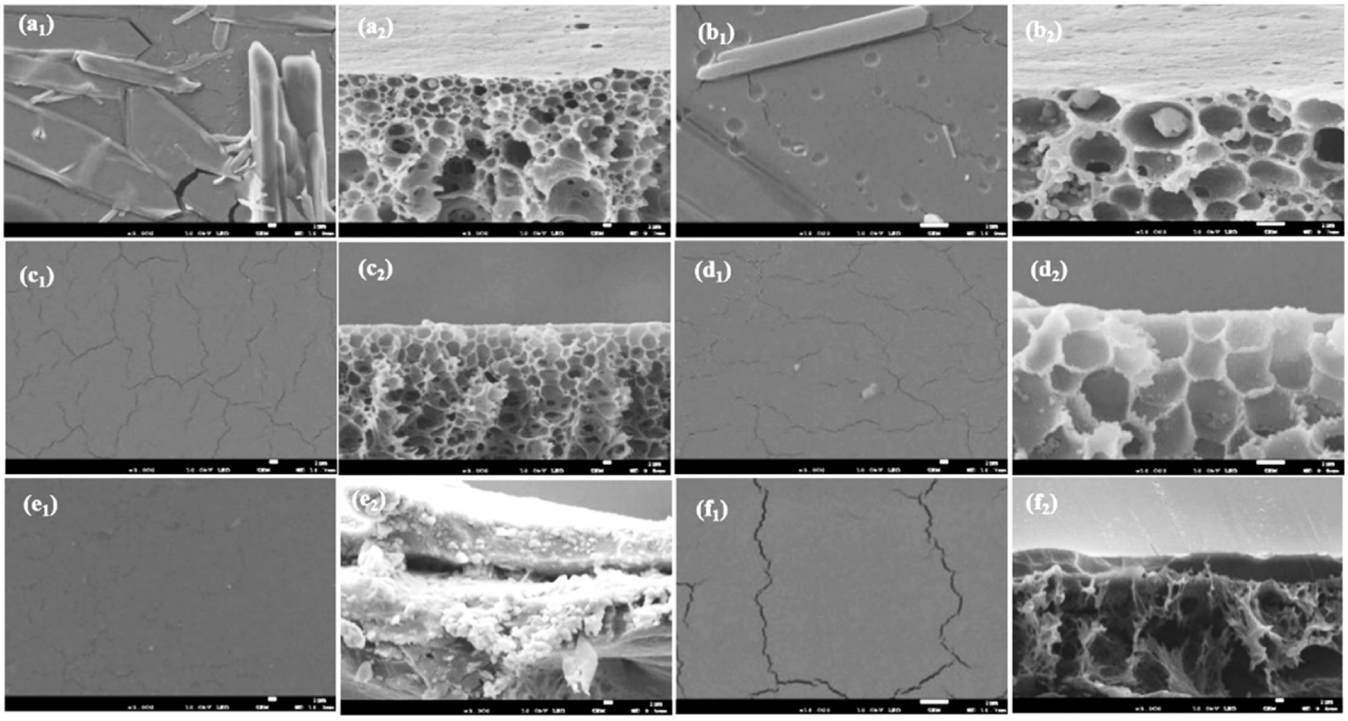

Fig. 8. Surface and cross-sectional structural SEM of PSU/epoxy substrate layers with different ratios 4:1 (a_1, a_2), 10:1 (b_1, b_2), 16:1 (c_1, c_2), 18:1 (d_1, d_2), 20:1 (e_1, e_2), & 22:1 (f_1, f_2).

selectively separable layer structure on its surface. Two long-chain carboxylic acid crosslinking agents, P(AA-AMPS) and P(SS-MA), both containing sulfonic acid groups, were selected to esterify and crosslink PVA. Esterification was conducted in a pH 1 solution at 100 °C, and after sufficient reaction, the separation layer of PVA no longer dissolved in hot water, maintaining a stable separation membrane structure. From the FTIR spectra in Fig. 4(a) and (b), new ester absorption peaks appeared after crosslinking, confirming the occurrence of esterification crosslinking reactions. The introduction of amino-crosslinked epoxy resin in the substrate layer, containing numerous –OH and –NH groups capable of reacting with –COOH, further enhances the interfacial bonding performance between the separation layer and the substrate layer. This has been further evidenced in the subsequent swelling stability tests. In the esterification crosslinking, distinct absorption peaks corresponding to C═O and C–O–C are evident, with two C–O stretching vibrations observed in the 1300 cm^{-1} to 1050 cm^{-1} region, serving as indicators for ester identification. The prominent absorption peaks observed in Fig. 4(a) and (b) provide clear evidence that both crosslinking systems undergo reactions with both PVA and the substrate layer (Fig. 5).

3.2. Thermal stability of separation layer

PVA serves as the central component in proving stable separation performance for the composite membrane. By introducing the P(SS-MA) and P(AA-AMPS) crosslinking systems, a more stable active separation layer can be achieved. Exemplifying with reference to the P(SS-MA) system, the TGA results of PVA before and after thermal crosslinking

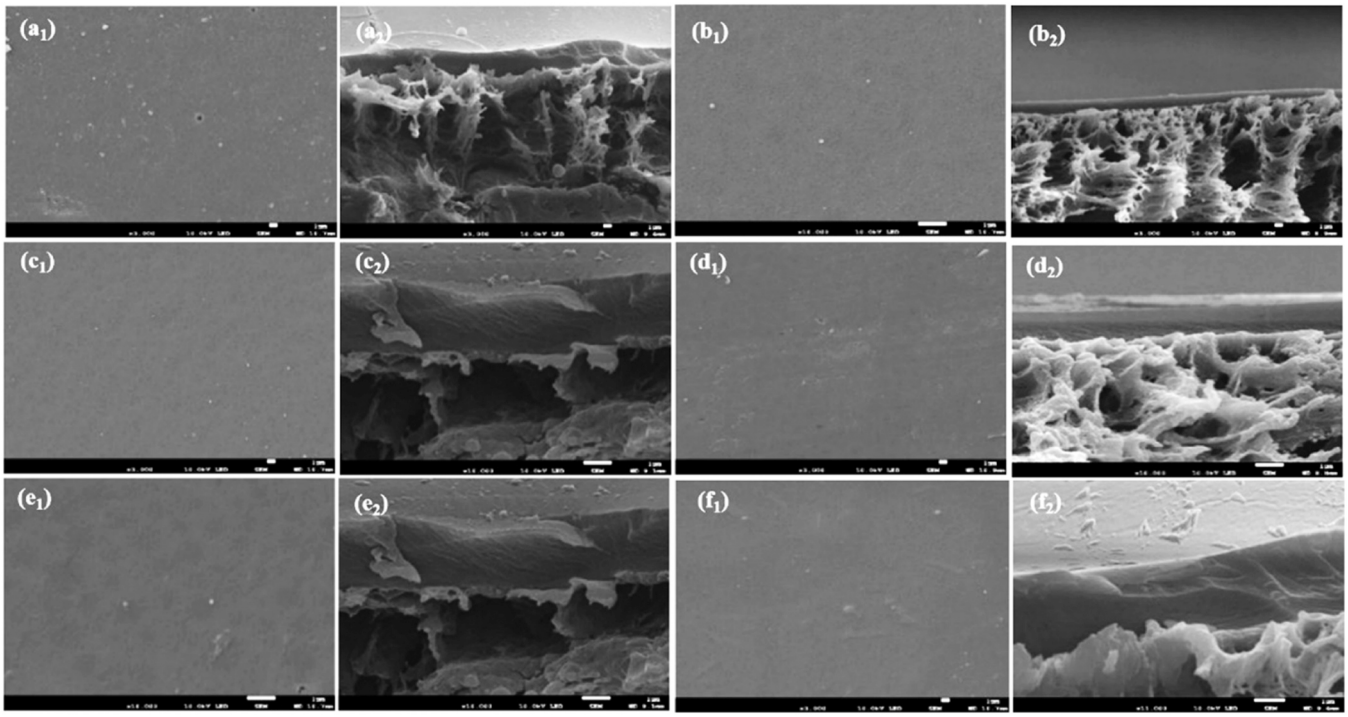

Fig. 9. Surface and cross-sectional structural SEM of PVA coated on different PSU/epoxy ratios 4:1 (a_1, a_2), 10:1 (b_1, b_2), 16:1 (c_1, c_2), 18:1 (d_1, d_2), 20:1 (e_1, e_2), & 22:1 (f_1, f_2).

Table 3
Pore size and porosity of PSU/epoxy (TEA) supporting membranes.

Membrane ID	Pore size (nm)	Porosity (%)
4:1	0.31	3.9
10:1	0.43	4.5
16:1	0.55	5.1
18:1	0.68	6.1
20:1	0.87	7.4
22:1	0.91	8.1

Table 4
Surface roughness of the PSU/epoxy (TEA) membranes.

Membranes	R_a (nm)	R_q (nm)	R_{max} (nm)
PSU/epoxy (TEA) substrate	7.40	10.9	3.26
PSU/epoxy (TEA) substrate at 100 ℃	14.0	18.1	189
PSU/epoxy (TEA) composite	1.55	2.18	2.34

at 100 ℃ are illustrated in Fig. 6, exhibiting roughly three distinct weight loss regions. Due to the inherent high hydrophilicity of PVA both before and after crosslinking, the system tends to absorb moisture from the air under room temperature conditions. Hence, the first region between 50 ℃ and 110 ℃ can be attributed to the loss of absorbed water molecules, with the pristine PVA showing lower weight loss due to increased water absorption resulting from a decrease in crystallinity after crosslinking. The second weight loss region, occurring between 110 ℃ and 210 ℃, is associated with the removal of side groups, including -OH groups, from the PVA polymer. The initially rapid weight loss of crosslinked PVA is attributed to the introduction of insufficiently reacted unstable groups by the crosslinking agent, which are more prone to removal than crystalline -OH groups under heating conditions. The third weight loss region is situated between 210 ℃ and 380 ℃ and correlate directly with the fracture of the ethylene groups in the main chain of PVA.

The weight loss rate of PVA/P(SS-MA) between 50 ℃ and 110 ℃ is 7.85 %, indicative of excellent water absorption characteristics. Subsequently, in the early stage of the second weight loss range, esterification or other functional groups in PVA/P(SS-MA) experience initial weight loss, maintaining an overall loss of approximately 12.41 %. Upon reaching 220 ℃, the pristine PVA and PVA/P(AA-AMPS) undergoes rapid weight loss earlier, while the stability of weight loss in crosslinked PVA with P(SS-MA) is maintained until 280 ℃. The third transition of crosslinked PVA with P(SS-MA) occurs between 280 ℃ and 460 ℃, arising from the thermal decomposition of the polymer main chain and the removal of -SO_3 groups. In contrast, the original PVA and PVA/P(AA-AMPS) experience complete degradation at 420 ℃, indicating a significant enhancement in the thermodynamic stability of P(SS-MA) crosslinked PVA.

3.3. *Effects of epoxy on the substrate layers*

Based on preliminary experiments, it was determined that the pure PSU substrate, formed through non-solvent phase transformation, exhibits a smooth surface with relatively low porosity. As depicted in Fig. 7 (a) and (b), when preparing a PVA crosslinked composite membrane on the surface of pure PSU, the surface's separation layer demonstrated susceptibility to detachment from the substrate layer of PV testing. Introducing bisphenol-A type epoxy resin into PSU at varying concentrations resulted in the transformation of the casting solution into a membrane through non-solvent phase conversion. Further, the epoxy resin underwent curing and crosslinking in the matrix facilitated by a crosslinking agent. Subsequently, a PVA crosslinked separation layer was applied to the surface of the obtained PSU/epoxy substrate. Water swelling stability revealed that the PV composite membrane, enhanced with added epoxy resin, displayed superior resistance to deamination compared to the substrate support layer without epoxy resin. In Fig. 7 (c)-(h), a surface comparison is conducted after 1 h of PV testing on PVA/PSU/epoxy PV composite membranes prepared with varying concentrations of epoxy resin.

For the TEA and HMDA crosslinking systems, we fabricated substrate

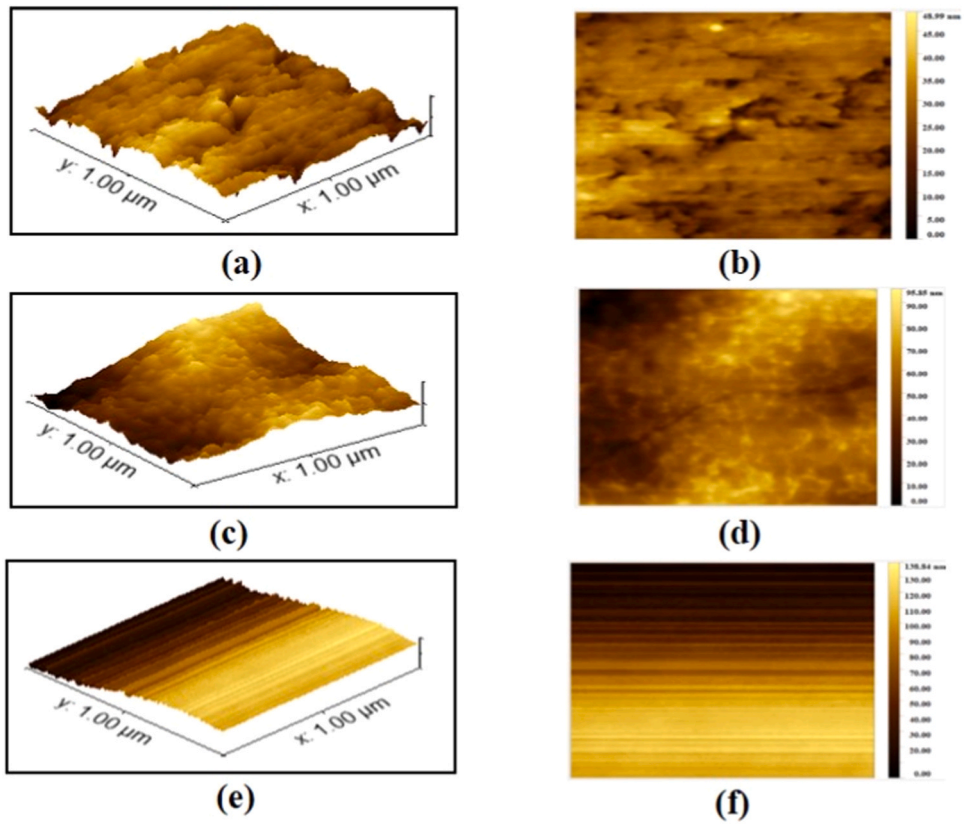

Fig. 10. The AFM images of the PSU/epoxy (TEA) (16:1) membrane: (a, b) 3D and 2D surface morphology of substrate layer at room temperature, (c, d) 3D and 2D surface morphology of substrate layer at 100 ℃, (e, f) 3D and 2D surface morphology of composite membrane at 100 ℃.

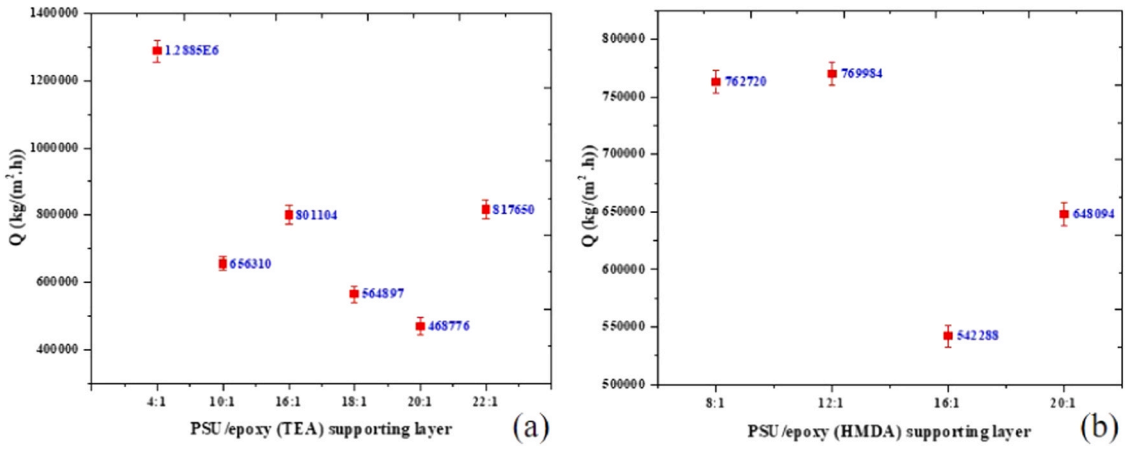

Fig. 11. Gas permeability of PSU/epoxy (TEA) and PSU/epoxy (HMDA) membranes with various proportions.

Table 5
Pure flux value of PSU/epoxy (TEA) composite membranes.

Membrane ID	Ratio	Water flux (kg $m^{-2}.h^{-1}$)
P/epoxy- 4	4:1	68.894
P/epoxy-10	10:1	81.758
P/epoxy-16	16:1	52.028
P/epoxy-18	18:1	62.220
P/epoxy-20	20:1	67.179
P/epoxy-22	22:1	66.321

structures with varying concentrations of epoxy resin. In the TEA system, the PSU/epoxy mass ratio ranged from 4:1–22:1. Experimental observations revealed that an augmentation in epoxy resin content resulted in increased surface roughness and a progressive thickening of the substrate layer film. Similar outcomes were obtained for the HMDA system. This suggests that the addition of epoxy resin influences the dynamic behavior of the casting solution undergoing non-solvent-induced phase transition, leading to alterations in the surface and cross-sectional structure of the PSU substrate layer. Following the preparation of a PVA separation layer on the substrate layer surface, extensive PV testing at 70 ℃ demonstrated that the incorporation of epoxy resin significantly enhances the binding stability of the PVA separation layer. This enhancement can be primarily attributed to the

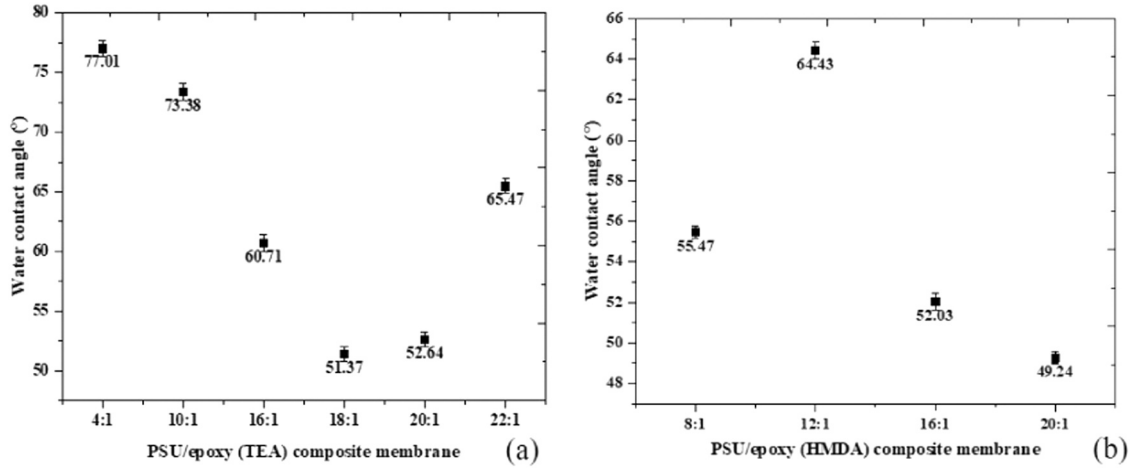

Fig. 12. Water contact angle of composite membranes with PVA/P(SS-MA) separation layer: (a) PSU/epoxy (TEA) and (b) PSU/epoxy (HMDA).

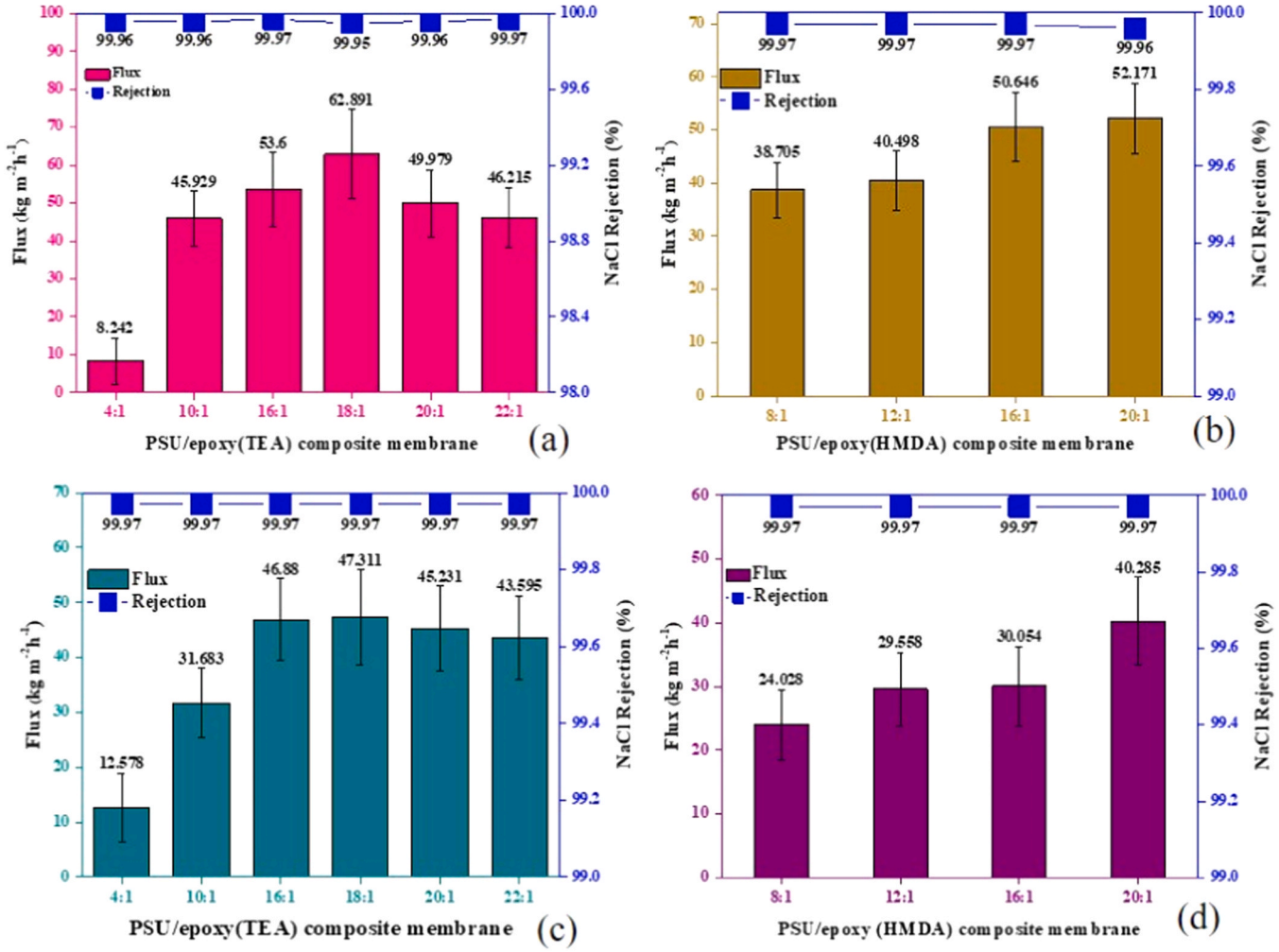

Fig. 13. Desalination performance of PSU/epoxy (TEA) and PSU/epoxy (HMDA) composite membranes with PVA/P(SS-MA) separation layer (a & b), desalination performance of PSU/epoxy (TEA) and PSU/epoxy (HMDA) composite membranes with PVA/P(AA-AMPS) separation layer (c & d) at 70 ℃.

increased presence of active groups such as -OH on the surface of the substrate layer, thereby improving hydrophilicity and surface binding performance. Additionally, there is a discernible improvement in PV test performance, a finding corroborated in subsequent experiments.

3.4. Morphological structure of composite membrane

The surface and cross-sectional morphologies of the PSU/epoxy (TEA) substrate layer and the PVA/PSU/epoxy (TEA) composite film were observed using scanning electron microscopy (SEM). As shown in

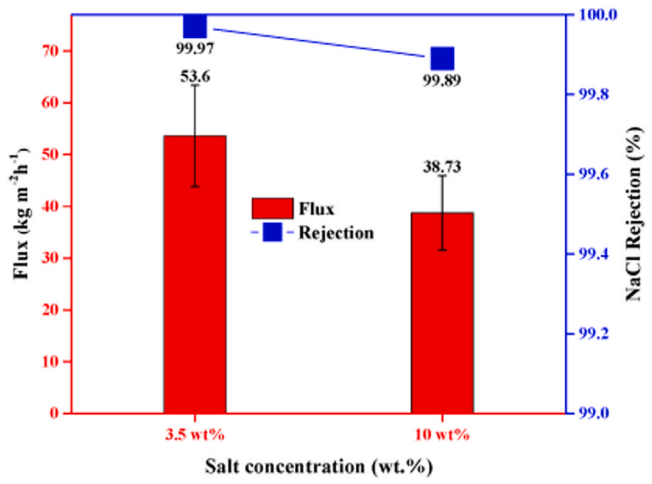

Fig. 14. Desalination performance of PSU/epoxy (TEA) composite membranes with various weight percentages of NaCl at 70 ℃.

Fig. 8, an increase in epoxy content led to an augmentation in the surface roughness of the substrate film (Khulbe KC). Additionally, porosity describes the part of a material volume that is made up of voids or pores. The pore structure in the cross-section underwent notable changes with the increasing epoxy content, displaying a characteristic asymmetric morphology, including a layered structure combining finger-like and sponge-like structures. In the cross-sectional images presented in Fig. 9, after coating the PVA solution on the substrate layer surface, a continuous layered structure was observed, rendering the surface smoother and more uniform.

Data on pore size and porosity suggest that increasing epoxy reduces these parameter as it acts as a binder and thickness the film. Table 3 shows that increasing epoxy resin results in a decrease in porosity and pore size. It is worth mentioning that the surface has a rough surface. It should be mentioned that the molecular structure of the cross-linked network can be affected by the interaction between the two simultaneous processes of phase separation and solidification, which may also have an impact on the fracture surface.

Through the analysis of AFM surface roughness tests before and after heat treatment of the PSU/epoxy (TEA) substrate layer, as well as after PVA coating, the average roughness (R_a), root mean square roughness (R_q), and maximum roughness depth (R_{max}) values are presented in Table 4. The AFM images, as depicted in Fig. 10, indicate a noticeable increase in surface roughness after heat treatment of the substrate layer. According to the Wenzel equation (GOOD, 1952), surface roughness significantly affects wettability, which can impact the effectiveness of PVA solution coating during conventional preparation processes. As shown in Fig. 10 (e), spraying a PVA solution containing P(SS-MA) crosslinking agent onto the surface of the substrate layer maintains good adhesion and markedly reduces the surface roughness during the preparation of the composite film. This suggests that the spray-coating process can produce a smooth, uniformly intact composite film.

3.5. The resistance of the substrate layer

The key characteristic of the substrate layer is to maintain stable support for the separation layer while allowing gases to pass through with low permeation resistance. Characterizing the overall porosity and permeability of the substrate layer can be achieved through gas permeability and water absorption tests, with a certain correlation between the two. The primary factors affecting gas permeation rate are thickness and operating pressure, as typically, permeability significantly decreases with increasing membrane thickness and then rapidly increase with an increase in operating pressure. Under a fixed pressure difference ΔP, N_2 permeation tests were conducted on PSU/epoxy (TEA) substrate layers with different mixing ratios to determine gas permeation resistance. The gas permeation resistance reflects the transport resistance of the composite film through the substrate layer permeation reaction. As seen in Fig. 11, with an increase in PSU content, the gas permeability in the system also significantly increases. This indicates a gradual increase in the permeable pore size in the substrate layer, weakening the resistance to permeating gases, consistent with the pore structure observed in SEM cross-sections. During desalination, water molecules are desorbed behind a dense selective layer of the pervaporation composite membrane, allowing them to penetrate the porous substrate as gaseous particles. Therefore, by identifying the gas transport characteristics of the substrate, it is possible to better understand the transport resistance of the composite film support layer. We checked the nitrogen flow rate of the membrane at different pressures because it is challenging to maintain a stable water vapor pressure. The tests also reveal a correlation between permeation resistance and the overall porosity of the substrate layer. Although the addition of PSU suppresses the pore size and surface roughness on the substrate layer's surface, the overall porosity of the matrix gradually increases, leading to an overall reduction in gas permeation resistance (Qin et al., 2022). A 22:1 mixing ratio may help improve the compatibility of PSU and epoxy components. Improved compatibility results in a more homogeneous membrane structure with fewer defects, enabling faster and more efficient gas transfer through the material. The PSU/epoxy (TEA) membranes' respective pure flux values are shown in Table 5. Among them, the PSU/epoxy (TEA) membrane with a 10:1 shows a higher flux than other proportions. The interaction between polymers in the membrane is affected by the ratio of PSU to epoxy resin. The ideal ratio of 10:1 between PSU and epoxy resin leads to better compatibility and intermolecular interactions in the membrane matrix.

3.6. The hydrophilicity of composite membranes

The purpose of water contact angle measurement (WCA) is to assess the wettability of a surface. By determining changes in the hydrophilicity of the PSU/epoxy layer surface, the cohesion and adhesion forces between the substrate layer surface and PVA molecules can be evaluated, thereby reflecting the strength of intermolecular interactions. Employing the same crosslinked PVA/P(SS-MA) separation layer on the surface of the substrate layer, water contact angles were measured on different composite film surfaces. The investigation revealed that distinct substrate layer structures exert a discernible influence on the

Table 6
Membranes and their performance in PV application for desalination.

Membrane	Feed type	Salt conc. (ppm)	Feed temperature (℃)	Flux (kg m^{-2} h^{-1})	Salt removal (%)	Ref.
PVA/PSU/epoxy (16:1)	NaCl solution	35,000	70	53.6	99.97	This experiment
c-GO/PEI-70k	NaCl solution	100,000	90	86.0	99.99	(Wang et al., 2022)
GO/PES	NaCl solution	30,000	60	47.8	99.9	(Almarzooqi et al., 2021)
GO/PAN	NaCl solution	100,000	90	65.1	99.8	(Liang et al., 2015)
MXene	NaCl solution	35,000	65	85.4	99.5	(Liu et al., 2018)
PVA/PSU hollow fiber	NaCl solution	30,000	71	7.4	99.9	(Chaudhri et al., 2015)
GOF	NaCl solution	35,000	90	11.4	99.9	(Feng et al., 2016)
PVA/PAN	NaCl solution	35,000	70	46.3	99.8	(Liang et al., 2018)

overall hydrophilicity of the composite membrane. WCA tests were conducted on PVA/PSU/epoxy systems in TEA and HMDA systems, as depicted in Fig. 12. Taking the TEA system as an example, composite membranes with PSU/epoxy ratios of 16:1, 18:1, and 20:1 exhibited pronounced hydrophilicity. The hydrophilicity of the composite membrane's surface, in turn, influence the overall water flux.

3.7. Pervaporation desalination performance

By varying the epoxy content in the substrate layer and employing TEA and HMDA as crosslinking agents for epoxy, two substrate layers with stable surface binding performance of PSU/epoxy were prepared. Subsequently, PVA active separation layers were fabricated on the surfaces of these two distinct substrate layers. The study compared the impact of two PVA esterification crosslinking agents, namely P(AA-AMPS) and P(SS-MA), on the desalination performance of the PV composite membrane. Desalination tests were conducted on 3.5 wt% NaCl saline solution under 70 ℃ conditions. Utilizing P(SS-MA) as the PVA crosslinking system, it was applied to the surface of the PSU/epoxy (TEA) substrate layer, and the PV results are depicted in Fig. 13 (a) and (b). The salt rejection rates for all composite membranes exceeded 99.9 %. This is primarily attributed to the increased epoxy content promoting the formation of a continuous sponge-like pore structure in the system, reducing the overall fully permeable porosity and thereby enhancing the overall permeation performance of the composite membrane. However, a further decrease in epoxy content results in the formation of a distinct asymmetric dense skin layer structure in the substrate layer. Previous experiments also demonstrated that an increase in epoxy content leads to an increase in membrane thickness, and the combined effects of these factors result in a decline in the overall gas permeation of the substrate layer.

During extended PV testing, both PVA separation layers exhibited excellent resistance to peeling and long-term stability within the PSU/epoxy ratios of 16:1 and 18:1. From Fig. 13 (c) and (d), it is evident in comparative experiments that the permeation flux values for the P(AA-AMPS) crosslinking agent are relatively lower than those for the P(SS-MA) crosslinking system. This discrepancy is primarily attributed to the hydrophilicity of the separation layer after PVA crosslinking, consistent with the results of contact angle testing. To validate the operational stability of the composite membrane in highly saline water, the desalination performance was compared under PSU/epoxy ratios of 16:1. Contrasting the PV performance under 70 ℃ conditions with 3.5 wt% and 10 wt% NaCl solutions, as shown in Fig. 14, it is evident that the permeation flux decreases under higher concentration conditions. This decline is primarily attributed to the intensified concentration polarization phenomenon during the dissolution and diffusion processes on the membrane surface in highly concentrated conditions, resulting in a reduction in the rate of water dissolution diffusion and subsequently causing as decrease in flux (Jarod M. Younker et al., 2013; Zavastin et al., 2010). However, the overall salt rejection performance can still be maintained at 99.89 %, demonstrating excellent salt rejection stability. Even though the data suggests that there is an upward trend in permeation flux of TEA-based substrate layer systems as the mixing ratio of PSU to epoxy gradually increases, it is critical to recognize the inherent measurement errors. The error bars accompanying our data show the range of variations in results that can be explained due to measurement errors or experimental variations. Given these uncertainties, the observed changes in permeate flux at different mixing ratios are not statistically significant. Adding the epoxy resin to the PSU just only increases the binding energy of the active layer and substrate layer, however, it cannot withstand long-term operation according to the error bar. Although the permeation flux of the composite membranes did not change significantly, the desalination rate can be maintained at more than 99.9 % when the mixing ratio of PSU to epoxy is gradually increased in the TEA-based substrate layer system.

Table 6 provides a comparative analysis of the desalination performance under different conditions for organic and inorganic membrane materials prepared by other research teams. In this experiment, the substrate layer of the PVA/PSU/epoxy composite film exhibited excellent interfacial binding performance with the separation layer. It maintained efficient permeation and desalination performance at 70 ℃, achieving a commendable level of performance in the context of organic substrate membrane systems. The straightforward preparation method makes it easily scalable for large-scale production of high-performance PV desalination membranes, establishing a robust foundation for PV desalination applications.

4. Conclusion

In the course of this innovative study, we augmented the adhesion resilience between the PSU substrate layer and the separation layer during the fabrication of PV desalination membranes by introducing epoxy resin into the casting solution. This inquiry substantiates the influence exerted by both quantity of epoxy resin and the distinct crosslinking systems TEA and HMDA on the surface topography and overall pore architecture of the PSU substrate layer. Through meticulous optimization, we secured the substrate layer's commendable support characteristics for the separation layer, ensuring heightened operational stability. Simultaneously, we attained elevated gas permeability for the substrate layer and superior performance in terms of pervaporation membrane functionality. Furthermore, a comprehensive analysis was undertaken to delineate the nuanced variations in the amalgamation of diverse PVA separation layer crosslinking systems with the substrate layer. Employing two disparate crosslinking agents, P(AA-AMPS) and P(SS-MA), for the preparation of PV composite membranes, we observed commendable interfacial adhesion and desalination efficiency. Notably, P(AA-AMPS) exhibited the highest water flux. While there were slight variances in water flux values for composite membranes employing distinct crosslinking agents, the salt rejection rates consistently surpassed the 99.9 % threshold. Consequently, the methodological advancements proffered in this study furnish indispensable guidance for the realization of prolonged operational stability in the deployment of PV desalination composite membranes within high-concentration saline desalination sectors.

Funding

This work is supported by Changzhou Key Laboratory of Biomass Green, Safe & High Value Utilization, NERC2404.

CRediT authorship contribution statement

Rui Zhang: Visualization, Supervision, Project administration. **Yunlong Xue:** Conceptualization. **Thi Thi Mar:** Writing – original draft, Resources, Investigation, Formal analysis, Data curation. **Jiahua Yan:** Conceptualization. **Bing Cao:** Supervision, Project administration. **Zijian Yu:** Conceptualization.

Declaration of Competing Interest

The authors declare that they have no known competing financial interests or personal relationships that could have appeared to influence the work reported in this paper.

Appendix A. Supporting information

Supplementary data associated with this article can be found in the online version at doi:10.1016/j.cherd.2024.04.052.

References

Acarer, S., 2022. Effect of different solvents, pore-forming agent and solubility parameter differences on the properties of PES ultrafiltration membrane. Sak. Univ. J. Sci. 26, 1196–1208.

Al Malek, S.A., Abu Seman, M.N., Johnson, D., Hilal, N., 2012. Formation and characterization of polyethersulfone membranes using different concentrations of polyvinylpyrrolidone. Desalination 288, 31–39.

Almarzooqi, K., Ashrafi, M., Kanthan, T., Elkamel, A., Pope, M.A., 2021. Graphene oxide membranes for high salinity, produced water separation by pervaporation. Membranes (Basel) 11.

An, W., Zhou, X., Liu, X., Chai, P.W., Kuznicki, T., Kuznicki, S.M., 2014. Natural zeolite clinoptilolite-phosphate composite membranes for water desalination by pervaporation. J. Membr. Sci. 470, 431–438.

Burts, K.S., Plisko, T.V., Bildyukevich, A.V., Li, G., Kujawa, J., Kujawski, W., 2022. Development of dynamic PVA/PAN membranes for pervaporation: correlation between kinetics of gel layer formation, preparation conditions, and separation performance. Chem. Eng. Res. Des. 182, 544–557.

Chaudhri, S.G., Chaudhari, J.C., Singh, P.S., 2018. Fabrication of efficient pervaporation desalination membrane by reinforcement of poly(vinyl alcohol)-silica film on porous polysulfone hollow fiber. J. Appl. Polym. Sci. 135.

Chaudhri, S.G., Rajai, B.H., Singh, P.S., 2015. Preparation of ultra-thin poly(vinyl alcohol) membranes supported on polysulfone hollow fiber and their application for production of pure water from seawater. Desalination 367, 272–284.

Cho, C.H., Oh, K.Y., Kim, S.K., Yeo, J.G., Sharma, P., 2011. Pervaporative seawater desalination using NaA zeolite membrane: mechanisms of high water flux and high salt rejection. J. Membr. Sci. 371, 226–238.

Eljaddi, T., Mendez, D.L.M., Favre, E., Roizard, D., 2021. Development of new pervaporation composite membranes for desalination: theoretical and experimental investigations. Desalination 507.

Feng, B., Xu, K., Huang, A., 2016. Covalent synthesis of three-dimensional graphene oxide framework (GOF) membrane for seawater desalination. Desalination 394, 123–130.

Gargol, M., Klepka, T., Klapiszewski, L., Podkoscielna, B., 2021. Synthesis and thermo-mechanical study of epoxy resin-based composites with waste fibers of hemp as an eco-friendly filler. Polymers (Basel) 13.

Good, R.J., 1952. A Thermodynamic derivation of Wenzel's modification of Young's equation for contact angles; together with a theory of hysteresis1. conttibution frox the research department, phosphate division. Monsanto Chemical Company 74, 5041–5042.

Guo, R., Fang, X., Wu, H., Jiang, Z., 2008. Preparation and pervaporation performance of surface crosslinked PVA/PES composite membrane. J. Membr. Sci. 322, 32–38.

Halakoo, E., Feng, X., 2020. Layer-by-layer assembly of polyethyleneimine/graphene oxide membranes for desalination of high-salinity water via pervaporation. Sep. Purif. Technol. 234.

Han, M.-J., 1999. Effect of propionic acid in the casting solution on the characteristics of phase inversion polysulfone membranes. Desalination 121, 31–39.

Hu, M., Cui, Z., Yang, S., Li, J., Shi, W., Zhang, W., Matindi, C., He, B., Fang, K., Li, J., 2021. Pregelation of sulfonated polysulfone and water for tailoring the morphology and properties of polyethersulfone ultrafiltration membranes for dye/salt selective separation. J. Membr. Sci. 618.

Jarod M. Younker, T.S., Hunt, Marcus A., Naskar, Amit K., Beste, Ariana, 2013. Pyrolysis Pathways of Sulfonated Polyethylene, an Alternative Carbon Fiber Precursor. J. Am. Chem. Sco. 135, 6130–6141.

Jin, F.-L., Li, X., Park, S.-J., 2015. Synthesis and application of epoxy resins: a review. J. Ind. Eng. Chem. 29, 1–11.

Julian, H., Nurgirisia, N., Qiu, G., Ting, Y.-P., Wenten, I.G., 2022. Membrane distillation for wastewater treatment: current trends, challenges and prospects of dense membrane distillation. J. Water Process Eng. 46.

Kaminski, W., Marszalek, J., Tomczak, E., 2018. Water desalination by pervaporation – comparison of energy consumption. Desalination 433, 89–93.

Kavanagh, J.M., Hussain, S., Chilcott, T.C., Coster, H.G.L., 2009. Fouling of reverse osmosis membranes using electrical impedance spectroscopy: measurements and simulations. Desalination 236, 187–193.

Khulbe K.C., F.C.a.M.T., Membrane characterization. Water and Wastwater Treatment Technologies.

Kılıç, Z., 2020. The importance of water and conscious use of water. Int. J. Hydrol. 4, 239–241.

Kim, S.-J., Oh, B.S., Yu, H.-W., Kim, L.H., Kim, C.-M., Yang, E.-T., Shin, M.S., Jang, A., Hwang, M.H., Kim, I.S., 2015. Foulant characterization and distribution in spiral wound reverse osmosis membranes from different pressure vessels. Desalination 370, 44–52.

Lee, K.P., Arnot, T.C., Mattia, D., 2011. A review of reverse osmosis membrane materials for desalination—development to date and future potential. J. Membr. Sci. 370, 1–22.

Li, L., Hou, J., Ye, Y., Mansouri, J., Zhang, Y., Chen, V., 2017. Suppressing salt transport through composite pervaporation membranes for brine desalination. Appl. Sci. 7.

Liang, B., Li, Q., Cao, B., Li, P., 2018. Water permeance, permeability and desalination properties of the sulfonic acid functionalized composite pervaporation membranes. Desalination 433, 132–140.

Liang, B., Zhan, W., Qi, G., Lin, S., Nan, Q., Liu, Y., Cao, B., Pan, K., 2015. High performance graphene oxide/polyacrylonitrile composite pervaporation membranes for desalination applications. J. Mater. Chem. A 3, 5140–5147.

Lim, Y.J., Goh, K., Kurihara, M., Wang, R., 2021. Seawater desalination by reverse osmosis: Current development and future challenges in membrane fabrication – a review. J. Membr. Sci. 629.

Liu, G., Shen, J., Liu, Q., Liu, G., Xiong, J., Yang, J., Jin, W., 2018. Ultrathin two-dimensional MXene membrane for pervaporation desalination. J. Membr. Sci. 548, 548–558.

Madaeni, S.S., Rahimpour, A., 2005. Effect of type of solvent and non-solvents on morphology and performance of polysulfone and polyethersulfone ultrafiltration membranes for milk concentration. Polym. Adv. Technol. 16, 717–724.

Mansur, H.S., Sadahira, C.M., Souza, A.N., Mansur, A.A.P., 2008. FTIR spectroscopy characterization of poly (vinyl alcohol) hydrogel with different hydrolysis degree and chemically crosslinked with glutaraldehyde. Mater. Sci. Eng.: C 28, 539–548.

Ong, Y.K., Shi, G.M., Le, N.L., Tang, Y.P., Zuo, J., Nunes, S.P., Chung, T.-S., 2016. Recent membrane development for pervaporation processes. Prog. Polym. Sci. 57, 1–31.

Park, S.-M., Jung, J., Lee, S., Baek, Y., Yoon, J., Seo, D.K., Kim, Y.H., 2014. Fouling and rejection behavior of carbon nanotube membranes. Desalination 343, 180–186.

Qin, D., Liu, H., Xiong, T., Wang, J., Zhang, R., Cao, B., Li, P., 2022. Enhancing the property of composite pervaporation desalination membrane by fabricating a less resistance substrate with porous but skinless surface structure. Desalination 525.

Tzanakakis, V.A., Paranychianakis, N.V., Angelakis, A.N., 2020. Water supply and water scarcity. Water 12.

Wang, Q., Li, N., Bolto, B., Hoang, M., Xie, Z., 2016. Desalination by pervaporation: a review. Desalination 387, 46–60.

Wang, Z., Sun, J., Li, N., Qin, Y., Qian, X., Xie, Z., 2022. Tuning interlayer structure to construct steady dual-crosslinked graphene oxide membranes for desalination of hypersaline brine via pervaporation. Sep. Purif. Technol. 286.

Xie, Z., Hoang, M., Duong, T., Ng, D., Dao, B., Gray, S., 2011. Sol–gel derived poly(vinyl alcohol)/maleic acid/silica hybrid membrane for desalination by pervaporation. J. Membr. Sci. 383, 96–103.

Yang, G., Xie, Z., Doherty, C.M., Cran, M., Ng, D., Gray, S., 2020. Understanding the transport enhancement of poly (vinyl alcohol) based hybrid membranes with dispersed nanochannels for pervaporation application. J. Membr. Sci. 603.

Zavastin, D., Cretescu, I., Bezdadea, M., Bourceanu, M., Drăgan, M., Lisa, G., Mangalagiu, I., Vasić, V., Savić, J., 2010. Preparation, characterization and applicability of cellulose acetate–polyurethane blend membrane in separation techniques. Colloids Surf. A: Physicochem. Eng. Asp. 370, 120–128.

Zeng, H., Liu, S., Wang, J., Li, Y., Zhu, L., Xu, M., Wang, C., 2020. Hydrophilic SPEEK/PES composite membrane for pervaporation desalination. Sep. Purif. Technol. 250.

Zhao, P., Xue, Y., Zhang, R., Cao, B., Li, P., 2020. Fabrication of pervaporation desalination membranes with excellent chemical resistance for chemical washing. J. Membr. Sci. 611.